CEAS Aeronautical Journal (2025) 16:377–398
https://doi.org/10.1007/s13272-024-00801-2

ORIGINAL PAPER

Using generic cities to assess flying ad-hoc network (FANET) performance

Tobias Marks[1] · **Konrad Fuger**[2]

Received: 8 March 2024 / Revised: 11 October 2024 / Accepted: 9 December 2024 / Published online: 1 February 2025

Abstract

Flying ad-hoc networks (FANET) offer a solution to provide communication among unmanned aerial systems (UAS) without ground infrastructure and, hence, may provide redundancy if main terrestrial communication systems fail. With a strongly growing UAS market, this redundancy is of particular importance especially if the vehicles are operated over densely populated regions, such as urban areas. To further develop the FANET technology, it is, therefore, essential to understand and predict the performance requirements for such networks and the necessary systems as they arise from the different applications. However, with the diversity of cities, the problem arises that custom-made simulation models often lack generality. For this reason, in our work, we introduce an approach to generate randomized cities and to model UAS traffic for selected applications to assess different performance metrics of the FANET. This approach comprises the creation of randomized city geometries, the derivation of UAS traffic demand on these geometries, as well as the simulation of the flights of each individual vehicle. To showcase the capabilities of the approach, we generate an exemplary city and obtain characteristic datasets of the UAS traffic which are then used to assess the FANET performance for a selected FANET application using a simplified network model. We will show that FANET performance is strongly influenced by the extent of the demand, demand distribution over time, vehicle speed, and delivery network geometry.

Keywords Ad-hoc network · Communication · Unmanned aerial vehicle

List of symbols

$\bar{\delta}$	Average UAS density at a specific timestamp
$\bar{\Delta}$	Aggregated UAS density of a scenario
η	Interval
τ	Overall accumulated flight time (min)
φ	Amount of UAS at a specific timestamp
$\bar{\Phi}$	Aggregated amount of UAS of a scenario
Φ_{max}	Maximum amount of UAS of a scenario
ρ	Population density ($1/km^2$)
ζ	Coverage
A	Area (km^2)
b	Common border length (m)
C	Center point
DT_{pd}	Set of departure times for package delivery
DST	Set of random destination points
e	Reachability at a specific timestamp
E	Reachability of a scenario
f_{pd}	Demand factor for package delivery
$\hat{h}_{max}$	Maximum number of hops at a specific timestamp
H_{max}	Maximum number of hops of a scenario
L_{E2E}	Maximum end-to-end delay budget (s)
l_{max}	Maximum per-hop delay budget at a specific timestamp (ms)
L_{max}	Maximum per-hop delay budget of a scenario (ms)
n_{pd}	Total package delivery demand
n_{ts}	Amount of time stamps
P	Population
r_c	Communication range (km)
r^u	Upper delivery range limit (km)
r^l	Lower delivery range limit (km)
r^S_{max}	Radius of the bounding circle
S	Set of all UAS

✉ Tobias Marks
tobias.marks@dlr.de

Konrad Fuger
k.fuger@tuhh.de

[1] Institute of Air Transport, German Aerospace Center (DLR), Blohmstr. 20, 20179 Hamburg, Germany

[2] Institute of Communication Networks (ComNets), Hamburg University of Technology (TUHH), Am Schwarzenberg-Campus 3, 20173 Hamburg, Germany

t	Simulation time (s)
$\bar{\tau}$	Average data rate at a specific timestamp ($kbps$)
$\bar{T}$	Average data rate of a scenario ($kbps$)
τ_{max}	Peak data rate at a specific timestamp ($kbps$)
T_{max}	Peak data rate of a scenario ($kbps$)

Indices

p	Population
g	Geographic
S	Scenario
D	District
B	Block

Abbreviations

A2A	Air-to-air
A2G	Air-to-ground
ADS-B	Automatic dependent surveillance-broadcast
AGL	Above ground level
AS	Airborne station
CBF	Contention-based flooding
DP	Droneport
FANET	Flying ad-hoc network
GBAS	Ground based augmentation system
GS	Ground station
LEO	Low earth orbit
LOS	Line-of-sight
MCDS	Minimum connected dominating set
MOCA	Minimum obstacle clearance altitude
PDF	Probability density function
UAS	Unmanned aerial system
UTM	Unmanned traffic management
VLL	Very low level
VTOL	Vertical take-off and landing

1 Introduction

1.1 Motivation

Flying ad-hoc networks (FANET) offer a solution to provide direct communication among unmanned aerial systems (UAS) without depending on available ground infrastructure. Among others, there are two main scenarios for which such FANETs are perfectly suited.

This is on the one hand the built-up of communication networks in areas lacking appropriate ground communication infrastructure (e.g., disaster areas or remote/undeveloped regions) and thereby enabling drone operations in the first place or providing wireless communication services for ground entities (see, e.g., [1, 2]).

On the other hand, a FANET provides for a redundant data link enabling, e.g., pilot drone communication or position reporting in structurally strong areas if main terrestrial communication systems fail.

Typically, UAS used for new applications (e.g., drone delivery [3], inspection services, and monitoring) only feature one single data link system to connect the vehicle to the ground. Hence, dangerous situations for people, other airspace users, or ground infrastructure can occur if this link fails. With the UAS market growing strongly in recent years and the new UAS applications becoming more and more popular, this redundancy is of particular importance especially if the vehicles are operated over densely populated regions, such as urban areas. Here, in the context of unmanned traffic management (UTM) and U-Space [4, 5], a backup communication system might even reduce safety-induced operational constraints, thus allowing for even new applications and business opportunities.

To further develop the FANET technology in urban areas, it is, therefore, essential to understand and predict the performance requirements for such networks and data link systems as they arise from the different applications, operational constraints (e.g., number and position of UAS in the air), and technological limitations (e.g., data rates and radio range).

While technological limitations can remain constant for different scenarios, the operational constraints strongly vary not only by the assessed application but also with the concrete city under examination as flight movements are strongly linked to the internal structure of the structure of the city.

With the diversity of cities, the problem arises that custom-made simulation models lack generality and, therefore, the obtained results may lose validity if transferred to other settings. With other words, the results obtained for a mid-size German city are not transferable to an U.S. mega city. This seems reasonable as population and size of both cities are very dissimilar. In general, population and size of cities strongly vary by income level, region, and more [6]. However, in addition to these, many other factors influence the operational constraints of UAS applications, such as for example the spatial distribution of population and buildings, centrality, and location of restricted areas. These additional factors can lead to the effect that even two mid-size German cities can result in completely different simulations in terms of flight movements resulting from UAS applications.

For this reason, in our work, we first present selected UAS and FANET applications and, based on these, we introduce an approach to generate generic cities by random processes and to model UAS traffic for these cities resulting from the selected applications to assess different performance metrics of the FANET independent of specific city geometries. In particular, our approach comprises the creation of randomized city geometries in terms of size, shape and internal structure and population distributions, the derivation of UAS traffic demand on these geometries, as well as simulating the flights of each individual vehicle using a simplified mobility model.

Using our method to create a set of varying city geometries and population distributions, we aim to achieve a more general insight into FANET performance than could be obtained by modeling a set of specific cities only. This insight is obtained by analyzing the relation between city specific parameters, flight demand, and the resulting mobility in combination with application-specific parameters and FANET performance. This flexible approach can be used in future works to derive more detailed technical performance requirements for the considered applications and technologies.

To showcase the capabilities of our approach, we generate an exemplary city and obtain specific spatial distributions of the demand for UAS flight movements. Based on this, we generate the corresponding individual flights. The thereby created mobility data are then used to assess FANET performance using a simplified network model. We show that our approach is suitable to link the demand for drone delivery to FANET assessment and point out key drivers that influence the performance of the FANET.

The works presented in this paper are results from the project VEREDUS that was funded by the German Ministry of Economic Affairs and Climate Action (Grant Agreement No. 20Q1939H). In the project, the focus was on the development of radios and antennas for direct drone-to-drone communication. Along with the hardware development, the assessment of the FANET performance using realistic mobility data was a major objective of the project. For further information, please refer to other project relevant publications [7–10].

1.2 State of the art

1.2.1 FANET

FANETs have been a hot topic in research for many years [11]. Nevertheless, much of the research has been focused on designing protocols or measuring channel models for FANETs. For example, [12] presents a survey of routing protocols applied in an FANET scenario, and [13] proposes a routing protocol specifically tailored to FANET. While these studies are important contributions, they use strongly simplified scenarios with only a very limited amount of UAS and simplified mobility models such as Gauss–Markov [14, 15], Random-Waypoint [16], or Smooth-turn [17] mobility. To improve on this, special mobility models have been proposed in [18, 19]. Still, the amount of UAS to expect and their spatial distribution remains undetermined which makes it impossible to derive communication requirements for FANET or evaluate the performance of protocols in realistic scenarios. Another approach was taken in [20] where well-established communication technologies were assessed based on their suitability to be used in UAS communication. But as only individual UAS were considered, the results have only limited applicability for the assessment of FANETs.

To get around the limitation of unknown UAS trajectories, researchers applied stochastic geometry to assess the performance of FANETs. In [7], communication requirements for large-scale FANETs were estimated using a 2D Poisson process with a constant spatial density to describe the positions of the individual UAS. A more elaborate method is applied in [2] where a post-disaster scenario is evaluated in which UAS are used as aerial base stations to provide coverage to users on the ground. Again, a uniform distribution of UAS on a 2D plane is assumed highlighting the need for more realistic mobility data.

1.2.2 UAS traffic and demand estimation

Drone delivery can be expected to be a major driver in logistics by replacing the last mile segment and enabling fast on time delivery. In the European Drones Outlook Study conducted by SESAR in 2017 [21], the potential for drone usage in Europe was already outlined from a market perspective. Since then, many companies already successfully introduced drone delivery services and operate the vehicles on a regular basis [22, 23]. However, demand prediction and traffic estimation for UAS flights in urban areas is a challenging research topic and has been addressed in several works. Here, the problem of identifying flights in the urban air mobility (UAM) domain is closely related to the problem of identifying flights for drone delivery. In both cases, estimations are usually based on population distribution and empirical data collected from other transportation modes for the applications under consideration (e.g., ground transportation or parcel delivery services). Here, the results are closely linked to the specific city or region under consideration.

Doole et al. [24, 25] estimate the demand for food and parcel delivery based on ground transportation data and derive the average amount of flights needed to deliver the eligible parcels in the metropolitan region of Paris. However, their approach can only derive total values for whole scenarios. UAS positions or local UAS densities as needed for FANET assessment are not derived. Borghetti et al. [26] use a similar approach to derive the number of parcels for Milan while they focus on the financial feasibility. Swaid et al. [27] model reasonable UAS movements for the city of Hamburg based on population distribution and local features. Kirschstein et al. [28] compare ground-based and drone delivery for the city of Berlin.

Also, in the domain of urban air mobility (UAM), many works model flight movements based on population and demand data derived form traditional sources. Hu et al. [29] model local air taxi flights based on taxi demand data for the city of Vienna as well as trips from the airport to the city.

1.2.3 City generation

The idea of creating generic cities based on procedural algorithms was followed in different domains (e.g., [30, 31]) while being used primarily for city planning and 3D visualization. Some works use generic cities in the assessment of UAS traffic impact (e.g., noise [32]) or identify vertiport locations for urban areas based on geometric patterns derived from general transportation axes (e.g., hexagonal pattern [33, 34]). However, most of the works use special selected cities for traffic modeling (e.g., Hamburg [27], Paris [24], or Milan [26]). Asmer et al. [35] present an approach to map cities to a circular shape and to distribute the population on a regular grid to make them comparable.

1.3 Our contribution

While all of these approaches yield interesting an reasonable results, due to the very specific nature of the local conditions of a city, the results are not necessarily transferable from one city to another. When it comes to the assessment of FANET performance, a more general approach is needed to relate flight demand to flight movements as FANETS can only operate properly if sufficient nodes are participating in the network and are adequately distributed in space. The number of nodes and their position, however, strongly depend on population distribution and city geometry. Here, our approach to create generic cities based on reduced city parameters can fill the gap between city specific use-cases and generic analytical modeling of FANETS as described in Sect. 1.2.1. An approach using generic cities to model urban package delivery drone traffic as presented in this work is not known to the authors.

2 Methodology

2.1 Assumption and general approach

In this work, we assume the FANET to be introduced in an urban environment, where high traffic densities are expected due to various use-cases, such as on-demand package/food delivery, delivery of blood/tissue samples, inspection of infrastructure, environmental or societal monitoring, and more. It is assumed that vehicles use the Very Low Level (VLL) airspace and weigh up to 25 kg as specified in [4, 5]. Larger vehicles, e.g., as used for air taxi services are currently not considered in our studies but can be envisioned, to be equally equipped with the communication systems in the future as they are likely to cross the VLL airspace to reach their vertiport.

There are two main operational parameters that determine the performance of an FANET. This is on the one hand the number of available nodes (airborne stations; AS) to establish the ad-hoc network along with their spatial distribution and on the other hand the communication range of the radio link. While a low number of AS or a sparse network might lead to connectivity problems, a high number of AS or a dense network can in turn lead to a congestion of the data link.

To investigate the influence of the aforementioned parameters on the FANET performance metrics, it is necessary to model the movement of the single vehicles in space and time. However, the movements should be as much as possible based on realistic assumptions. Each city is highly individual and bears its own special boundary conditions. Hence, results for a particular city might not be transferable to other cities.

Therefore, in our approach as shown in Fig. 1, we simulate flight movements for generic cities that are generated using specific creation rules. For these cities, a demand for UAS package delivery flights is created, and in a next step, individual missions are generated based on this demand. The single flights are simulated using an agent-based simulation

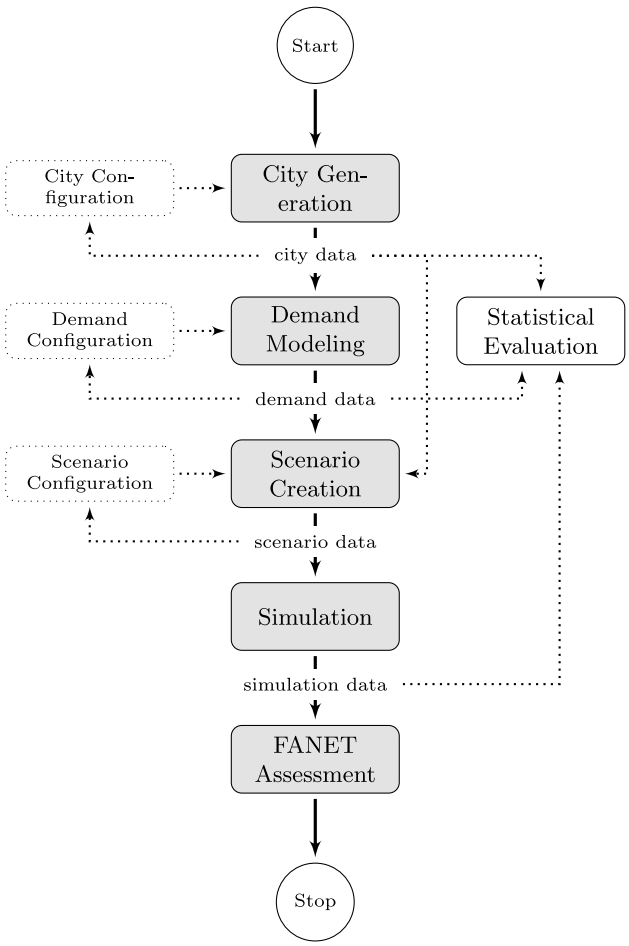

Fig. 1 General approach as followed within this work

environment and based on the resulting 4D-trajectory data the FANET performance is assessed. To match a specific city type, business model, or CONOPS, all aforementioned steps are highly customizable in our simulation environment.

2.2 Metrics

In this section, the metrics used in our work to assess cities, UAS movements, and FANET performance will be presented.

2.2.1 City metrics

Basic city structure

In general, we describe a city by a set of *blocks* of population that are grouped into *districts*. The geographical limitation of the city during the city creation process is referred to as the *limiting polygon*. The outer geographical extent of the city constituting the area covered by blocks is referred to as the *outer polygon* of the city. In the following, brief definitions are given for the single elements.

Blocks

Blocks are geographical areas within the city with a defined population assigned to them.

Districts

Districts are consolidated blocks that are forming a larger unit. Districts are used to assign delivery centers to them that deliver packages within the district boundary.

Limiting polygon

The limiting polygon of a city describes the limits in which blocks are placed during the city creation process.

Outer polygon

The outer polygon of a city describes the limits of the area that is covered by blocks after the city was created and unsuitable blocks, that exceed the block size limits (e.g., maximum/minimum size, maximum perimeter length), are removed.

City metrics

A whole city and parts of cities such as blocks or districts can be characterized by basic metrics. These are area, population, and population density [6]. Of course, real cities are much more complex; however, in the context of our basic model approach, only these three parameters will be used to characterize a city.

Area

The area of the city or parts of a city (blocks, districts) is given by the geographic area covered by the selected entity independent of the population within its boundaries. The area of the whole city or scenario is depicted by A^S. Areas of districts and blocks are denoted as A^D and A^B accordingly. For a whole city, the mean district and block sizes are denoted as $\bar{A}^D$ and $\bar{A}^B$

Population

The total population of a city or parts of a city are denoted as P. The population of the whole city or scenario is referred to as P^S the population of a district as P^D and of a block as P^B.

Population density

The average geographic density of the population of the scenario ρ^S is the population P^S per area A^S

$$\rho^S = \frac{P^S}{A^S} \tag{1}$$

Radius of the bounding circle

The radius of the bounding circle of the city $r^S_{\max}$ can be calculated using the outer polygon of the city. As no flight activity will take place outside of this circle, the diameter of the circle can be interpreted as the upper range limit for the data link. Data links with higher ranges will not lead to better performance of the FANET.

2.2.2 UAS traffic metrics

UAS amount

To assess the FANET, the active nodes of the network are relevant (see Sect. 2.8) independent of whether they are in flight or not.

Amount of active/airborne UAS

The amount of active UAS at a specific time $\varphi(t)$ is given by the cardinality of the set of active UAS $S(t)$. The amount of airborne UAS will be denoted as $\varphi(t)'$ accordingly

$$\varphi(t) = \mid S(t) \mid . \tag{2}$$

Aggregated amount of active/airborne UAS

The *aggregated amount* of active UAS $\bar{\Phi}$ for a whole scenario can be calculated by summing up $\varphi(t)$ over all timestamps n_{ts} of the respective scenario and dividing it by the number of timestamps, respectively. The aggregated amount of airborne UAS will be denoted as $\bar{\Phi}'$ accordingly

$$\bar{\Phi} = \frac{1}{n_{ts}} \sum_{n_{ts}} \varphi(t). \tag{3}$$

Maximum amount of active/airborne UAS

The maximum amount of active UAS occurring during a scenario is accordingly denoted as $\Phi_{\max}$. The maximum amount of airborne UAS will be denoted as $\Phi'_{\max}$ accordingly

$$\Phi_{\max} = \max(\varphi(t)). \tag{4}$$

UAS densities

There are several ways to define UAS density. Dahle et al. [36] propose to use simultaneous flights per km^2 as density metric. However, as there might be more or less UAS in the airspace during the day, UAS density is highly dependent on time. We, therefore, additionally distinguish between the local

density $\delta(x, y, t)$, the average density $\bar{\delta}(t)$, and the aggregated density $\bar{\Delta}$ as defined below. Densities for the whole scenario, distinct blocks, or districts can be derived accordingly.

Local geographic UAS density

One means of calculating the *local geographic density* $\delta_g(x, y, t)$ is by applying an appropriate kernel function to the geographic location (x, y) of each UAS at a time t and summing up over the simulation area. The local geographic density can only be estimated correctly if individual 4D-trajectories of the single flights are known.

Average UAS density

The *average density* $\bar{\delta}(t)$ is the amount of UAS in the air $\varphi(t)$ at time t divided by A^S for the average geographic density $\bar{\delta}(t)_g$ and divided by P^S for the average population density $\bar{\delta}(t)_p$

$$\bar{\delta}(t)_g^S = \frac{\varphi(t)}{A^S} \quad \bar{\delta}(t)_p^S = \frac{\varphi(t)}{P^S}. \tag{5}$$

Aggregated UAS density

We define the *aggregated density* $\bar{\Delta}$ by dividing the aggregated UAS amount $\bar{\Phi}$ by a reference value. Hence, we define the aggregated density per geographical area $\bar{\Delta}_g$ to be the aggregated amount of UAS in the air $\bar{\Phi}$ divided by the area of the given scenario A^s. Hence, $\bar{\Delta}_g$ corresponds to the metric proposed by Dahle et al. [36]. The aggregated density per population $\bar{\Delta}_p$ is accordingly defined by the aggregated amount of UAS in the air $\bar{\Phi}$ divided by the population of the given scenario P^s

$$\bar{\Delta}_g^S = \frac{\bar{\Phi}}{A^S} \quad \bar{\Delta}_p^S = \frac{\bar{\Phi}}{P^S}. \tag{6}$$

2.2.3 FANET metrics

To establish an FANET, communication equipment and protocols must be used that conform to the requirements of the network. In this chaptern we define the metrics we use to assess the FANET performance.

Communication range/number of hops

One of the most critical metrics for FANET is the communication range r_c of the wireless data link. Depending on the spatial distribution of AS, a certain range is needed to obtain a connected network. For communication over multiple hops, the communication range also determines how often data have to be forwarded from its source to its destination. We denote the maximum number of hops that is required by a message sent by AS i at time t to traverse the whole network as $h^i_{\max}(t)$. The maximum number of hops occurring at timestamp t is denoted as $\hat{h}_{\max}(t)$ and given by

$$\hat{h}_{\max}(t) = max(h^i_{\max})(t). \tag{7}$$

The maximum number of hops occurring in the whole scenario $H_{\max}$ is given by

$$H_{\max} = \max(\hat{h}_{\max}(t)) \tag{8}$$

accordingly.

Reachability

The reachability E is a metric to assess how good network wide data exchange can be performed based on the topology of the network. The reachability $e^i(t)$ of an AS i at time t is defined as the number of data packets that actually reach the AS $n_{\text{rec}}(t)$ divided by the total number of data packets that *could* reach it $\phi(t) - 1$

$$e^i(t) = \frac{n^i_{\text{rec}}(t)}{\varphi(t) - 1}. \tag{9}$$

The average reachability at time t is denoted as $e(t)$ and given by

$$e(t) = \frac{1}{\varphi(t)} \sum_i e^i(t). \tag{10}$$

The aggregated reachability of a whole scenario is accordingly given by

$$E = \frac{1}{n_{ts}} \sum_t e(t). \tag{11}$$

As we consider communication over multiple hops in our study, the reachability is mainly driven by the connectivity of the network. Therefore, we study E depending on the communication range. It has to be noted that E forms an upper bound of the ratio of packets that can be received. In reality, the packet reception ratio will be lower as packets are lost due to channel noise, obstacles in the transmission path. or packet collisions. Nevertheless, the reachability is an important metric to assess the minimum required communication range to facilitate network wide information exchange.

Data rate

Another crucial performance metric is the required data rate. For every UAS, this is the sum of the data rate required to send out its own data and to receive and forward data from other UAS through the network. The data rate of AS i at time t is then denoted as $\tau^i(t)$. The peak data rate at time t is denoted as $\tau_{\max}(t)$ and given by

$$\tau_{\max}(t) = \max(\tau^i)(t); \tag{12}$$

we calculate $T_{\max}$ as the highest data rate that is required by an individual UAS at any time during the study according to

$$T_{\max} = max(T_{\max}(t)). \tag{13}$$

For the average data rate $\bar{T}$, we assume all data traffic to be evenly distributed among all UAS. While this is an important metric to dimension any communication system, it does not show the full picture as individual UAS might require a substantially higher data rate for short periods of time. The average data rate at time t is given by

$$\bar{\tau}(t) = \frac{1}{\varphi(t)} \sum_i \tau^i(t), \tag{14}$$

while the aggregated data rate for the whole scenario is given by

$$\bar{T} = \frac{1}{n_{ts}} \sum_t \bar{\tau}(t). \tag{15}$$

Delay budget

Finally, we define the delay budget $L^H_{\max}$ as the maximum delay of a data packet that can be incurred on a hop, so that the data are still delivered on time to its destination. This is calculated by dividing the maximum end-to-end delay allowed by a FANET application L_{E2E} by $H_{\max}$

$$l_{\max}(t) = \frac{L_{\text{E2E}}}{\hat{h}_{\max}(t)} \tag{16}$$

$$L_{\max} = \frac{L_{\text{E2E}}}{H_{\max}}. \tag{17}$$

2.3 UAS applications

While the radio range of the communication system can be assumed to remain constant, it is crucial to define the appropriate UAS applications as they strongly influence the node density of the ad-hoc network. There are many future and current UAS applications starting from package delivery over inspection and surveillance, to photography, film, and more. However, it is assumed that the delivery of goods is expected to be a major driver for the use of UAS in the near future, leading to a large number of aerial vehicles operating in urban areas throughout the business hours. Therefore, to assess the performance and limitations of the FANET, this application was selected as the focus of our work.

2.3.1 Business case

Companies already use UAS for last mile delivery on a daily basis with strong business cases in highly populated urban and metropolitan areas [23], widely separated suburbs, or remote places (e.g., [37]). Benarbia et al. [3] and Kellermann et al. [38] give a good overview of current research on the topic of drone package delivery. While other studies (e.g., [24] or [25]) differentiate between package delivery and food delivery, in our study, we assume that both are just two different aspects of the drone delivery use case. Recent developments of operational drone delivery networks show that food companies and resellers team up together and feed the droneports with the products right in place (e.g., [22]).

Furthermore, it is assumed that drone delivery takes place within a 12 h period between 8 a.m. and 8 p.m. which is in line with current drone delivery operating hours. For non-uniform distributions, we assume the peak to be located at 2 p.m. representing a higher demand for package delivery around noon (e.g., due to increased food or drink deliveries).

2.3.2 Vehicles

There are plenty of different vehicles suitable for package delivery. As the vehicle characteristics strongly influence the whole traffic scenario, for our studies, we defined two vehicles (see Table 1), one multicopter and one hybrid UAS (fixed wing with VTOL capabilities) based roughly on commercial drone delivery services already in operation.

2.3.3 Summary

In the following, we briefly summarize the UAS application we investigate in our work.

- Package delivery application for food, parcels, and more.
- One drone delivery network performing UAS operations for multiple customers (e.g., food-chains, grocery stores, and resellers).
- No delivery takes place in close vicinity to the stations (walking distance).
- Droneports are placed throughout the city to reach a certain amount of the population within a delivery district.
- Only one type of VTOL-UAS (see Table 1) is in operation.
- Demand is distributed uniformly or Gaussian over the operating hours of the scenario.
- Demand is depending on population and is immediate.
- Cruise altitude is assumed to be 120 m AGL for all UAS.
- Delivery period of 12 h (from 8 a.m. to 8 p.m.).

Table 1 Vehicle characteristics

Param.	Vehicle	
	A	B
Type	Multicopter	Hybrid
Lat. speed	10 m/s	29 m/s
Clb./desc. speed	3 m/s	3 m/s
Max rnd. trip dist	20 km	20 km
Max del. range (r^u_{pd})	8.5 km	8.5 km

2.4 FANET applications

UTM is an important topic for the future of UAS. While early system proposals were designed based on a few central entities monitoring the airspace, granting flight permissions and providing separation services, recently much of the research has focused on decentralized approaches to UTM [39]. Here, position information and intents are shared among all entities in the network allowing for faster and more resilient decision-making. In the VEREDUS project, we identified two main UTM applications for the projected FANET. This is on the one hand the provision of a situational overview for both UAS as well as ground entities and on the other hand the provision of a control connection in case of primary link loss. However, once an FANET is in place, it provides the basis to use it for additional applications [e.g., Ground Based Augmentation System (GBAS) service, approach assistance to drone ports or providing telecommunication services for ground entities in disaster areas [1, 2]]. As the situational overview is deemed to create substantially more data traffic than the control connection it will be used for the FANET assessment (see Sect. 2.9). However, both applications will be briefly described in the following.

2.4.1 Situational overview

As the skies are getting more and more crowded, it is essential and mandatory to provide up-to-date information on vehicles' identities, positions and intentions. The collected information can be used by authorities to manage air traffic flows, deconflict/adapt single flights or by the vehicles themselves to enable collision avoidance tasks and self-separation. The FANET can be used to provide the necessary information by flooding the network with messages, such that all nodes as well as ground entities can reconstruct an overview of the current situation [similar to automatic dependent surveillance-broadcast (ADS-B) or flight alarm (FLARM)]. This application thereby allows for the U-Space traffic information and network identification services [40].

To simulate this FANET application, several assumptions are made. First of all, a refreshment rate of the situational overview of 5 s was assumed that is roughly aligned with ICAO requirements for radar systems [41]. Furthermore, a data rate T_F of 1.6 kbps was assumed based on the MAVLINK common message set [42] and the airborne ADS-B transmission rate [43]. This means that new packets are emitted every 0.5 s. If the information in the previous packet should never be older than 5 s for any node in the network, the end-to-end delay budget L_{E2E} is 4.5 s. If a refreshment rate of 5 s is achieved for any node in the network, nearby nodes experience a much higher refreshment rate which is beneficial for collision avoidance. Depending on the operational constraints, [44] shows that a detection range between 150 m and 500 m is required for UAS on a collision course and, therefore, UAS must be separated by this distance at all times. To account for the position uncertainty that arises between the reception of position updates, this range must be increased accordingly. With that, the update interval has a direct influence on the permissible density of UAS in the airspace.

2.4.2 Control connection

The second main application for the FANET is the provision of a redundant control connection between operator and vehicle in case of primary connection (e.g., via terrestrial telecommunication systems) loss that is independent of any ground infrastructure. An additional satellite connection can be considered as a backup in the case that the FANET is not available. However, high latencies and costs might limit the use of satellite connections in the future. Based on the MAVLINK common message set [42], the data rates for this application can be assumed as 100 bps for the downlink (T_{PD}, ground station to airborne station) and 1500 bps for the uplink (T_{PU}, airborne station to ground station). The maximum end-to-end delay L_{E2E} is assumed not to exceed 1 s.

2.5 City generation

In this section, the process of city generation is presented beginning with an overview of the creation process in general. In the following sections, the single steps are presented in more detail. An exemplary city creation can be found in Sect. 3.

2.5.1 General approach

Figure 2 shows the general approach for creating a city in our work. First, a fixed number of blocks are generated following a specific distribution rule. If the population and size satisfy the desired specification, in a next step, blocks are grouped into districts that constitute a delivery region. If the setting provides for the required coverage, the city geometry is fixed and can be used to derive a corresponding demand. Based on the demand, the single connections and flights are being generated, which are subsequently simulated to obtain the UAS positions for the final FANET assessment.

2.5.2 Block distribution

Blocks are generated by randomly or orderly placing points on a plane and if applicable within a desired region (limiting

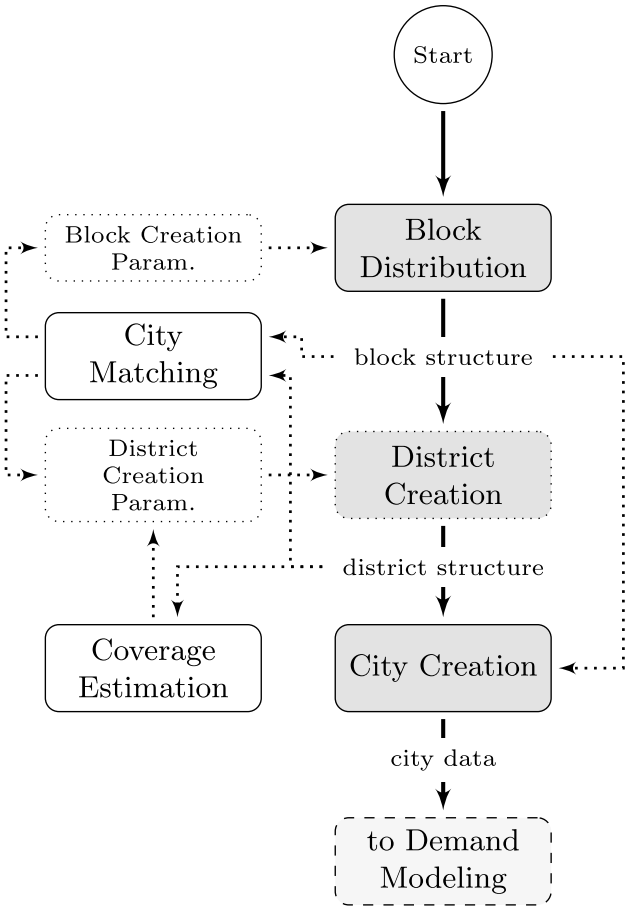

Fig. 2 Schematic flow of city generation

polygon). In a next step, these points are used to construct a Voronoi diagram. Each of the thereby created Voronoi regions is considered a block and is assigned either a fixed or a random population. In a next step, the center of area is calculated for each block and assigned to it. To avoid large or even infinite blocks, all blocks larger than a specific threshold or with outlines longer than a specified limit are removed from the set.

Figure 3 shows examples of different block distributions using different creation methods. In grid mode (a), blocks are placed in an equidistant grid, whereas in uniform mode (b), blocks are placed randomly following a uniform distribution. In multivariate mode (c), blocks are distributed randomly following a multivariate Gaussian distribution. In all cases, the final outline of the city can additionally be limited to a desired limiting polygon as shown exemplarily for the city of Hamburg (d). Here, the outer polygon of the city (red) is closely matching the limiting polygon (blue) used in the city creation process.

After the blocks are created, the basic city parameters (area and population) can be derived and used to the match desired values if necessary.

In our study, we choose the multivariate creation method to create the example city (see Sect. 3.1).

2.5.3 District derivation

The geometric optimal shape of a delivery district would be a Voronoi diagram based on the locations of the droneports, such that flight distances are minimized. However, it can be expected that due to a multitude of factors (e.g., business decisions, regulations, and available sites), the delivery areas will deviate from that optimum. Therefore, in our approach, delivery districts are derived by randomly choosing a block as origin of a new district and expanding it by adding adjacent blocks (that exceed a minimum common border length $b_{\min}$) until the thus created district meets the minimum requirements or exceeds the upper limits. Here, the limits can be given by either population $(P^D_{\min}, P^D_{\max})$, or area $(A^D_{\min}, A^D_{\max})$. If a district cannot continue to grow further, and does not meet the minimum requirements, it is added to another adjacent district. If all blocks are assigned to districts in a next step, the centers of area C^D_a as well as the center of area weighted by population in the blocks C^D_p are being calculated for each district and assigned to it. The basic algorithm of this process is depicted in Algorithm 1.

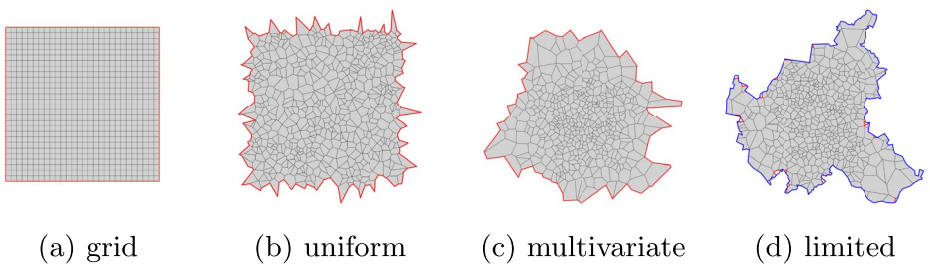

Fig. 3 Resulting block distributions for different creation modes (outer polygon, red; limiting polygon, blue)

Algorithm 1 District creation

```
input : block data
while not all blocks are assigned to districts do
    randomly select block B from unassigned blocks
    assign B to new district D
    calculate metrics for D
    while A^D ≤ A^D_max and P^D ≤ P^D_max do
        while not all blocks are tested do
            randomly select block B' from unassigned blocks
            if B' is adjacent to D then
                calculate common border length b_DB'
                if b_DB' ≥ b_min then
                    add B' to D
                    recalculate metrics for D
                    break
                end
            end
        end
        if no block can be added to D then
            if A^D ≤ A^D_min or P^D ≤ P^D_min then
                while not all districts are tested do
                    randomly select district D' from districts
                    if D is adjacent to D' then
                        calculate common border length b_DD'
                        if b_DD' ≥ b_min then
                            add D to D'
                            recalculate metrics for D'
                            break
                        end
                    end
                end
            end
            break
        end
    end
end
```

2.5.4 Coverage estimation

As districts are interpreted as delivery regions for packages, the weighted center C_p^D of each district is selected as a droneport (DP). Other positions for the DP (e.g., C_a^D or random) are also easily possible. In our solution, the packages are delivered from this DP to all destinations within the district and within range. Hence, the distribution of DPs determines the coverage ζ_{pd} of the city by the package delivery service. Depending upon the operation range of the UAS, the coverage can be calculated. We refer to the operation range as upper limit of the delivery range r_{pd}^u, whereas the lower limit r_{pd}^l is defined as the range around each DP in which no delivery is expected due to economic reasons. Depending on the business case, it can be reasonable to assume that packages can be delivered from one DP close to another (e.g., different operating companies). However, in our work, we assume that all DPs are operated by one company, so that drone delivery close to another DP or into another delivery district is not intended. In this case, coverage needs to be determined on a district basis. The district coverage $\hat{\zeta}_{\text{pd}}^D$ is defied by the area within the district covered by the service A_{pd}^D divided by the district area A^D. Hence, the total district-based coverage of a city results to

$$\hat{\zeta}_{\text{pd}} = \frac{\sum_i A_{\text{pd}}^{D_i}}{\sum_i A^{D_i}}. \tag{18}$$

2.6 Demand modeling

Flight demand is assumed to be based on population and due to the UAS applications considered to be immediate. This means that if there is demand for a flight, it is conducted immediately. This should not be mistaken with the initial demand created by the customer, when he or she orders a package. However, the main purpose of a drone delivery network in cities is to deliver as quick as possible. Hence, it can be assumed that the gap between customer demand and flight demand is minimized.

To distribute the flight demand over the day, we assume a specific distribution function. In our study, we use either a Gaussian or uniform distribution, while the limits of this distribution are confined assuming UAS operations during usual business hours only (night flight restriction).

Demand is then generated based on the population of a district by calculating the total number of flights and assigning a demand time based on the distribution function. The amount of demand is represented by the demand factor for package delivery f_{pd}. The total flight demand for package delivery n_{pd} in number of flights for a district D is then calculated by

$$n^D_{\mathrm{pd}} = \lceil f_{\mathrm{pd}} \cdot P^D \rceil. \tag{19}$$

The demand is then distributed over time creating a set of demand times DT^D_{pd}, so that

$$n^D_{\mathrm{pd}} = \mid \mathrm{DT}^D_{\mathrm{pd}} \mid \tag{20}$$

is fulfilled. Based on the city structure and the demand times for the districts, in the next step, connections are established that satisfy the demands. Connections are created within the delivery range (upper range limit r^u_{pd} and lower range limit r^l_{pd}) and selected based on density of the blocks following a probability rule.

First, a set of random destination points DST that are located within a delivery district is created. Next, the population density of the blocks ρ^B at the particular destination points is determined and associated with the destinations. For all destination points, population densities are then normalized according to

$$\rho'^B_{\mathrm{DST}_i} = \frac{\rho^B_{\mathrm{DST}_i}}{\sum_j \rho^B_{\mathrm{DST}_j}} \tag{21}$$

and distributed over the interval [0, 1) so that

$$\eta_i = \left[\sum_i \rho'^B_{\mathrm{DST}_{i-1}}, \sum_i \rho'^B_{\mathrm{DST}_i} \right) \tag{22}$$

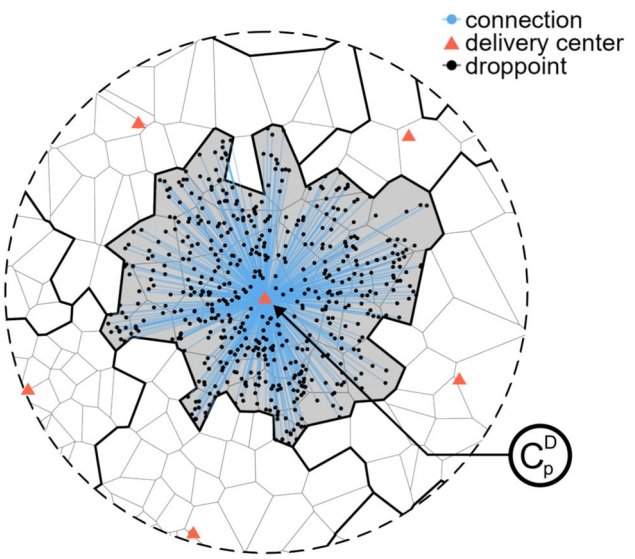

Fig. 4 Creation and selection of connections based on population density ($f_{\mathrm{pd}} = 0.003$), district boundary, and weighted district center C^D_p

is fulfilled. For each demand time in DT, a random number in the interval [0,1] is then generated. The particular destination DST_i is subsequently selected by identifying the appropriate interval η_i. By this method, connections to higher populated blocks are preferred. A comparison of Figs. 10 and 15 shows that the created demand pattern matches the population distribution.

It needs to be noted that multiple simultaneous demands even using different district structures or other distribution modes can easily be overlaid in our simulation. However, as future UAS business models and CONOPS are highly speculative in this work, we focused on one single demand pattern to reduce complexity of the results.

2.7 Scenario creation

Based on the city geometry, the flight demand, and the connections, the final scenario is created. This means that for each flight, a specific mission is generated departing at the specific demand time from the assigned DP. The missions can then be simulated using the chosen UAS performance model. To create the missions for the use case of package delivery, it is assumed that the UAS are departing from a DP located at C^D_p of a district and radially delivering the

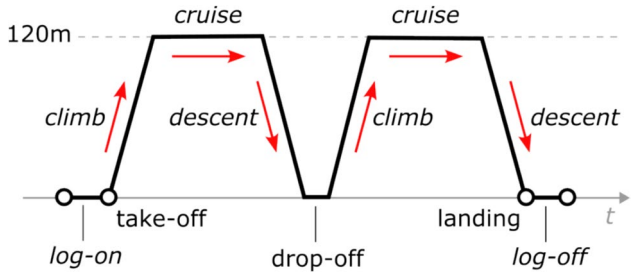

Fig. 5 Schematic activity/flight profile of UAS over time

packages into the district. Here, direct connections between DP and delivery destination are assumed (Fig. 4). To take into account the duration of the delivery process, a (randomized) period of maximum 120 s is added to the mission if the delivery destination is reached.

2.8 Simulation of UAS movement

In our study, we use a simplified model for UAS movement on which the vehicles are moving with constant speed along the flight path. However, more advanced point mass models featuring controllers for altitude, speed, and course are currently being developed.

Furthermore, we assume a VTOL multicopter or hybrid type of aircraft to perform the missions using a simplified flight profile, that is described in the following and presented in Fig. 5.

Before take-off, the data link is initialized and the UAS logs on to the network. It is assumed that the duration of this process is between 20 and 40 s. After take-off at the assigned DP, the AS climbs vertically until the desired altitude is reached (in our study, we assume 120 m). After reaching this altitude, the UAS switches to cruise phase flying at a constant speed toward the destination. If the destination is reached, the UAS stops the horizontal movement and descents vertically until touch-down. Then, after a random period of time that is assumed to let the customer unload the package, the UAS takes off again. The duration of this unloading is assumed to be between 60 and 120 s. Next, the UAS climbs to its assigned altitude again and returns to the DP it originated from accordingly. After landing the UAS logs off from the network and shuts down the data link. Again, the duration of this process is assumed to be between 20 and 40 s.

In our analysis, we use two different vehicles as depicted in Table 1. However, simulations with multiple vehicle types operating in parallel featuring different parameters are easily possible within our simulation environment, but are not considered in this study due to complexity reasons.

It needs to be noted that active nodes in the FANET are not necessarily airborne, e.g., if the drone lands to unload its package. In our simulation, the drone becomes active as soon as the take-off time is reached until it touches down on the DP after the mission. Data link initialization and cancelation times were not covered by our study but are intended to be considered in future works.

2.9 FANET assessment

To evaluate the impact the resulting UAS trajectories have on the performance of the established FANET, we selected the situational overview as the most demanding FANET application. The reasons for this are twofold: First, the situational overview must be active at all times and for all UAS, while the redundant control connection is only active in case of a loss of the primary control connection. Second, the data exchanged for the positional overview must be delivered to every other UAS, while the data for the control connection must only be delivered to the operator of a given UAS. Therefore, the positional overview requires a considerable higher data rate and creates stricter delay budgets.

2.9.1 Simulation of broadcast trees

To obtain the required performance of the FANET, we simulate the necessary data exchanges for the situational overview. For this, we create snapshots of the mobility at regular time intervals. Every snapshot is then transformed into a graph representation where every UAS represents a vertex of the graph and an edge between two vertices is created if the distance between the corresponding UAS is lower than the communication range r_c. This process is repeated for a wide range of r_c.

On each of these graphs, a search is executed for each UAS as the sender of data to identify all other UAS that have to forward the data, so that it is delivered to all (reachable) UAS. The schedule describing the succession in which UAS forward data is called a Broadcast Tree.

The most efficient way to obtain such a broadcast tree is to calculate the minimum connecting dominating set (MCDS) of the graph. Nevertheless, due to the computational complexity, data exchange over the MCDS cannot be realized in real mobile networks. Therefore, we implemented a graph search that could actually be realized in the real world. To do so, we draw inspiration from contention-based flooding (CBF) [45]: Here, efficient forwarding of data is achieved by introducing a contention mechanism, that prefers forwarders that are located far away from the sender (Fig. 6). In our graph search, we emulate this process by first selecting a start vertex and adding all its neighbors to a contention list. Next, we sort the contention list descending by distance to the sender. For each vertex in the contention list, we execute

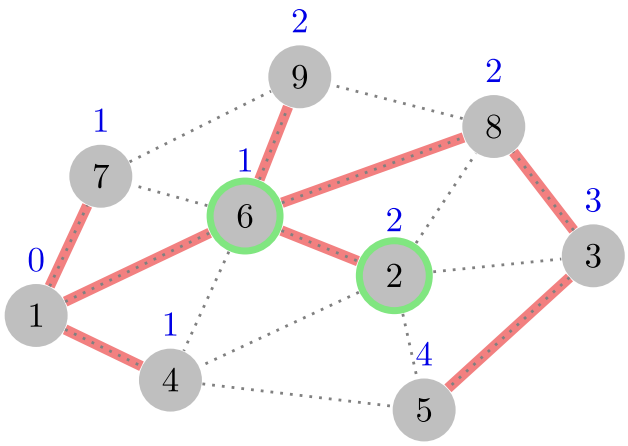

Fig. 6 Schematic of contention-based flooding; MCDS (green); broadcast tree created by CBF (red); step number of CBF creation (blue)

a “transmission" by taking its neighbors and removing them from the contention list if they were previously in it or adding them to a new contention list otherwise. This process is repeated until no further vertices can be reached.

2.9.2 Analysis of FANET metrics

The process of obtaining Broadcast Trees is executed for every UAS is a snapshot. In doing so, we count the number of transmissions until the search terminates, the number of consecutive forwarding stages and the number of vertices reached. Taking the maximum number of consecutive transmissions as $H_{\max}$, we calculate $L_{\max}$. As the broadcast tree includes all forwarders, we can obtain the required data rate for each UAS and calculate $\bar{T}$ and $T_{\max}$. The reachability E is calculated as the number of UAS reached divided by the total number of UAS. Repeating this for every timestep results in a time series of the respective metrics.

3 Results

The results are presented in three sections. In the first section, the city generation will be demonstrated using an exemplary city. In the second section, an aggregated analysis will be presented showing the dependency of the metrics on city parameters. Finally, in the third section, the analysis of the resulting FANET assessment will be presented.

3.1 City creation results

In this section, the city generation will be demonstrated using an exemplary city. Parameters for district size are assumed in anticipation of results presented in Sect. 3.1.3.

3.1.1 Matching city metrics

To showcase how the approach presented in this paper can be used to match existing cities in terms of population and size the city of Hamburg was selected. In a first step, it is important to match the main city metrics P and A. In Fig. 7 the main German cities are shown as defined by their areas and populations, respectively. It can be seen that especially for the largest cities Berlin, Hamburg, Munich, and Cologne, the values strongly differ, while the values for smaller cities lie closer together.

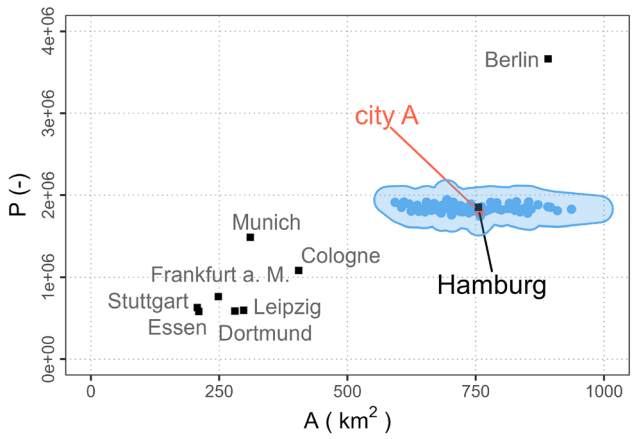

Fig. 7 Size and population of major German cities. City A matching area and population of the city of Hamburg

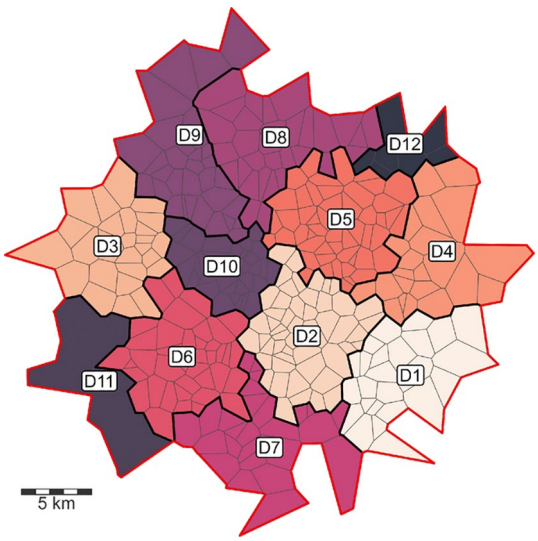

Fig. 8 City geometry of city A. Districts are depicted in different colors. ($P = 1800828$, $A = 757.6km^2$); outer polygon (red)

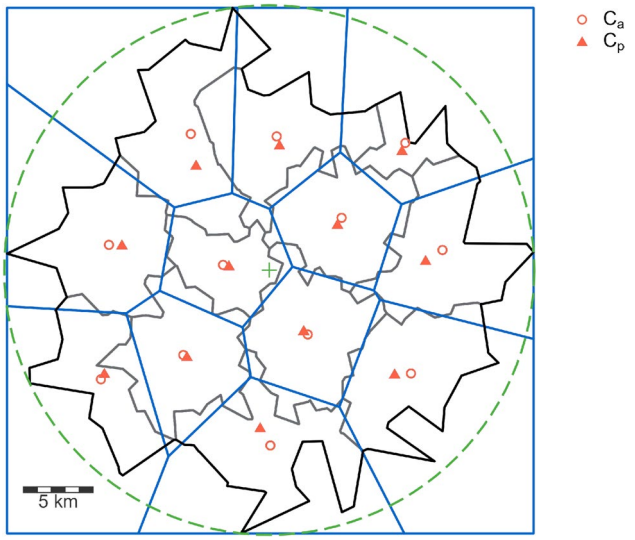

Fig. 9 City geometry of city A. Bounding circle (green, $r^S_{\max} = 19062$ m) and Voronoi regions calculated from C^D_a (blue)

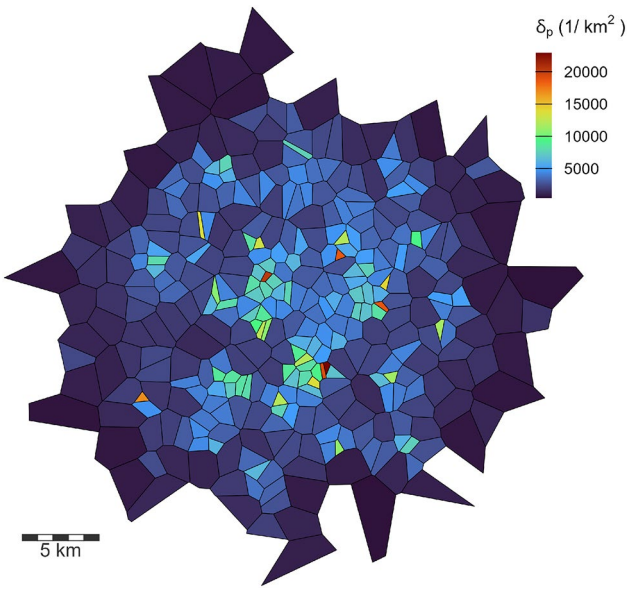

Fig. 10 Resulting population density of blocks of city A

In a next step, we varied the generation parameters of our city creation model to match the values of Hamburg. Figure 7 shows the resulting values for a set of randomly created cities with varying population and area. It can be seen that while the variation of the population is considerably small, the area shows a higher variation. This is due to the fact that there is no geographical limitation to the extent of the city, while the population is more restricted by the number of blocks and the population assigned to it. Thus, the variation increases with the random selection

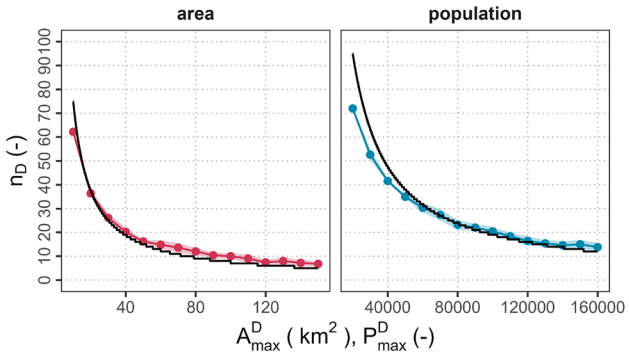

Fig. 11 Dependency of number of districts on maximum district size $A^D_{\max}$ and maximum district population $P^D_{\max}$ (based on 5 samples per setting)

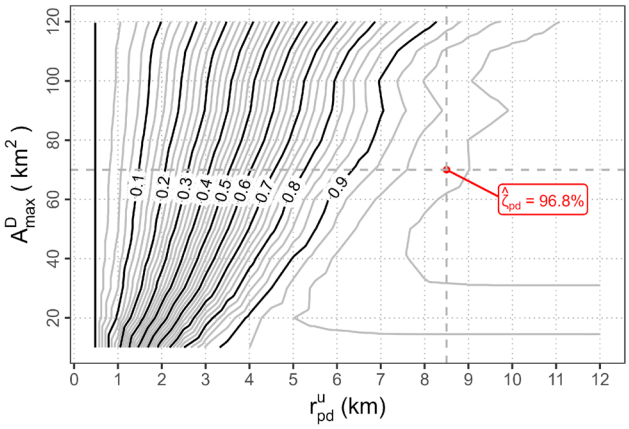

Fig. 12 Dependency of package delivery coverage $\hat{\zeta}_{\text{pd}}$ on maximum district size $A^D_{\max}$ and package delivery range r^u_{pd}

of sample points. However, our model provides the possibility to contain the city creation to an exact polygon (limiting polygon). This way, the area of the projected city can be matched much better or even to the exact desired outline of the city under examination (see Sect. 2.5.2). For our example, we select the sampled city from the set that is best matching the values for Hamburg ($P_{\text{ham}} = 1852478$, $A_{\text{ham}} = 755.09$ km^2) for further evaluation and refer to it as city **A**.

Figure 8 shows the block and district structure of city A (assuming $A^D_{\max} = 70$ km^2). It can be seen that the blocks are smaller in the center, while the districts that are created based on area size are equally distributed over the city. The area of the generated city is limited by the outer polygon shown in red (no limiting polygon was used during the creation).

In Fig. 9 for each district, the positions of the centers are shown. It can be observed that the centers weighted by population C^D_p are considerably shifted with relation to the

area centers C_a^D. The figure also shows the resulting Voronoi areas using C_a^D for tesselation. The district boundaries created by the district creation process basically match the Voronoi boundaries. However, the Voronoi areas represent the ideal case for packet delivery to minimize flight distances from C_a^D. In contrast, the randomly created district borders account for uncertainties, e.g., due to local conditions or business decisions and hence introduce a level of variation that can be assumed to better represent real conditions.

Figure 10 shows the resulting population density of city A. Due to the multivariate Gaussian distribution of the block points and the partly random population assignment to the blocks, the population density is higher in the center of the city as here blocks turn out to be smaller. At the outskirts of the city the blocks are considerably large resulting in less population density.

3.1.2 Determining number of districts

As discussed in Sect. 2.5.3, the size of delivery districts can be based on both population and area. Figure 11 shows a plot of the number of districts n_D as obtained from our model versus the maximum district size $A^D_{\max}$ (left) and maximum district population $P^D_{\max}$ (right). It can be observed that in both cases the algorithm is basically matching the theoretically calculated number of districts (black curves).

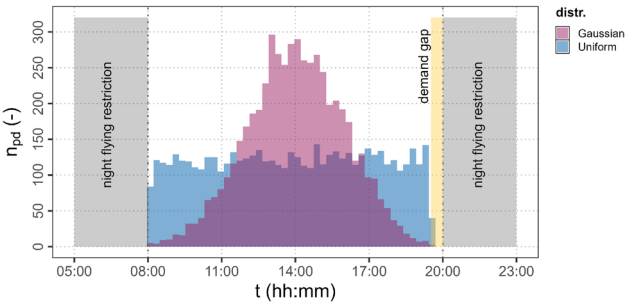

Fig. 14 Resulting demand distributions for city A for uniform and Gaussian distribution types ($f_{\text{pd}} = 0.003$)

3.1.3 Matching coverage

The number of districts is strongly influencing the coverage of the city by drone delivery, as in each district a delivery center is placed in the population center C_p^D. Using the maximum delivery range r^u_{pd}, the coverage $\hat{\xi}_{\text{pd}}$ for package delivery can be calculated. Figure 12 shows a variation study of $\hat{\xi}_{\text{pd}}$ depending on $A^D_{\max}$ and r^u_{pd}. The plot shows the average of 5 samples that were calculated for each parameter combination.

Based on these results, the necessary district size limitation for a desired coverage and/or range can be extracted from the plot. In our example, we choose a maximum district size of $A^D_{\max}$ of 70 km^2 for city A (as indicated within Fig. 12) exhibiting a high coverage for the assumed delivery range r^u_{pd} of 8.5 km.

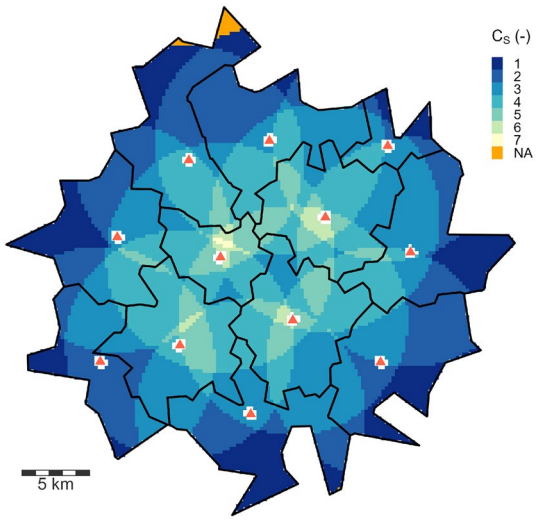

Fig. 13 Resulting package delivery coverage C_S (DPs in range) for city A ($A^D_{\max} = 70\,\text{km}^2$, $r^u_{\text{pd}} = 8.5\,\text{kmm}$)

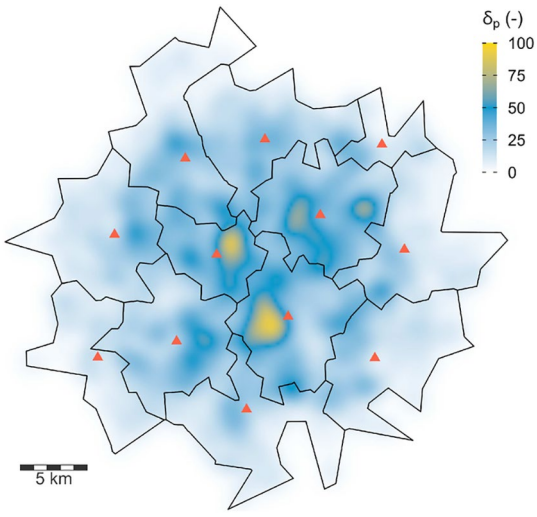

Fig. 15 Exemplary resulting drop point density for city A ($f_{\text{pd}} = 0.003$)

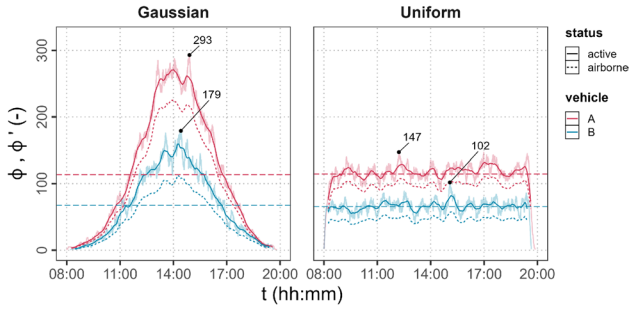

Fig. 16 Number of active AS over time $\varphi(t)$, $\Phi_{\max}$ and $\bar{\Phi}$ as well as AS $\varphi(t)'$ (dashed) for demand factor $f_{\text{pd}} = 0.003$ and both vehicles A and B

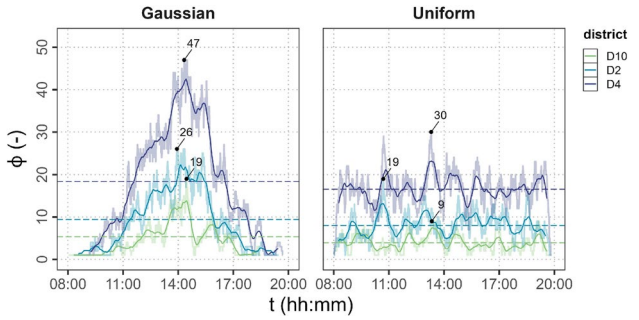

Fig. 17 Number of active AS over time $\varphi(t)$ for demand factor $f_{\text{pd}} = 0.003$, vehicle A and 3 selected districts

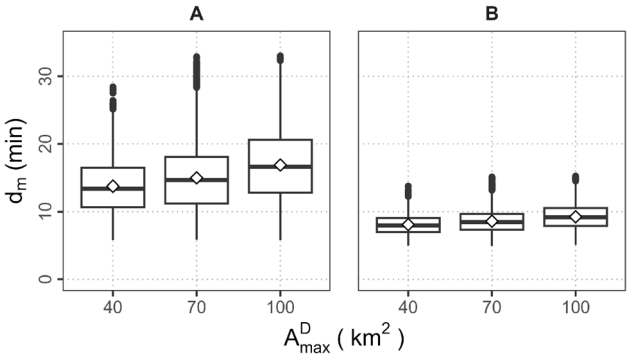

Fig. 18 Boxplot of mission time d_m for scenarios with changing $A^D_{\max}$ and vehicles A and B ($f_{\text{pd}} = 0.003$, 1 sample per setting, Gaussian distribution)

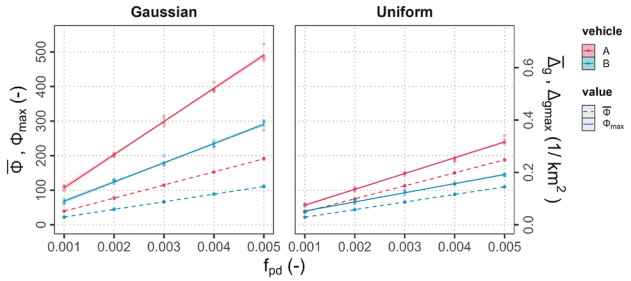

Fig. 19 Linear fit for $\Phi_{\max}$, $\bar{\Phi}$ (left axis), $\bar{\Delta}_g$, Δ_{gmax} (right axis) against demand factor f_{pd} for both vehicles and Gaussian and uniform distribution. (Note: based on five samples per setting)

For this setting, a district structure (see Fig. 8) for city A is then generated that will be used in the subsequent studies. Figure 13 shows the coverage for city A and the assumed district structure for the selected setting ($A^D_{\max} = 70\,\text{km}^2$ and $r^u_{\text{pd}} = 8.5$ km). It can be seen that the whole area is well covered by at least one DP, while (especially in the center) strong overlapping of the delivery areas occur. Only a small area in the north of the city remains uncovered.

3.1.4 Demand and scenario creation results

Based on the demand settings in the next step, the flight demand is created for city A as presented in Sect. 3.1. Here, the demand distribution over time can be set using distribution functions and can be limited by operating hours. Assuming a maximum mission duration d_m, the demand creation is limited to shortly before reaching the late constraint to have no active flights after this limitation left. As discussed in Sect. 2.6, the demand factor f_{pd} regulates the amount of demand based on population. The demand is then assigned to each district based on the particular population amount.

In our study, we varied the demand factor to achieve different values for $\bar{\Phi}$ and $\Phi_{\max}$ and thereby link the FANET performance to the demand. Figure 14 shows the distribution of the flight demand over the operating hours ($f_{\text{pd}} = 0.003$) as well as for both uniform and Gaussian distribution. The limitation by night flying restrictions are shaded gray, whereas the demand gap before the later limit is shaded yellow.

Each flight demand is then translated into a delivery network (see Sect. 2.7). Figure 4 shows exemplarily the delivery network resulting from a fixed demand ($f_{\text{pd}} = 0.003$) for one district. The density of the drop points for the whole scenario and city A is shown in Fig. 15. When comparing to the population distribution in Fig. 10, it can be seen that the created drop point density matches the population distribution of the city very well.

3.2 Simulation results

In this section, the results of the simulations for city A while using the settings derived in the previous sections are presented.

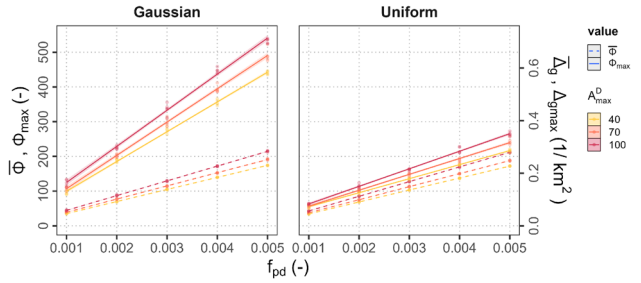

Fig. 20 Linear fit for Φ_{max}, $\bar{\Phi}$ (left axis), $\bar{\Delta}_g$, Δ_{gmax} (right axis) against demand factor f_{pd} for different maximum district sizes A^D_{max} and Gaussian and uniform distribution. (Note: based on five samples per setting; vehicle A)

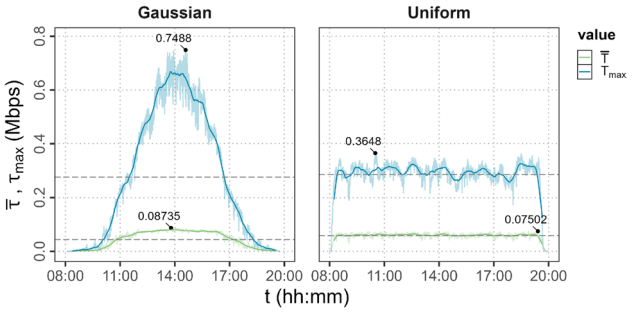

Fig. 21 Exemplary time series for $\bar{\tau}(t)$ and $\tau_{max}(t)$ ($r_c = 4\,km$; $f_{pd} = 0.005$; vehicle A)

Table 2 Predicted f_{pd} values for desired aggregated UAS densities $\bar{\Delta}_g$ and Φ_{max} (vehicle A)

$\bar{\Delta}_g$	Distribution	f_{pd}	Φ_{max}	Distribution	f_{pd}
1.0	U	20.1	1000	U	20.4
	G	19.9		G	9.7
5.0	U	100.8	5000	U	103.2
	G	99.7		G	48.6

3.2.1 Time series analysis

Figure 16 shows the resulting number of active vehicles $\varphi(t)$ (solid line) as well as airborne vehicles $\varphi(t)'$ (dashed line) over the simulation time for Gaussian and uniform demand distribution as well as both vehicles A and B (see Table 1). The maximum amount of UAS Φ_{max} as well as the aggregated amount of UAS $\bar{\Phi}$ are marked for all scenarios.

It can be observed that the number of active vehicles drastically differs between uniform and Gaussian demand distribution. While the average values remain similar, the maximum values of the Gaussian distribution are significantly higher. The number of airborne vehicles is lower, due to the time needed for unloading on ground, the moving average curves show an almost constant offset.

Figure 17 shows the number of active vehicles per district (three example districts). It can be observed that the curves basically follow the distribution of the whole scenario, however, with stronger variation. For a particular DP, the maximum number of active UAS equals the minimum amount of UAS needed to satisfy the demand in our model. More vehicles are needed if times for charging and battery/payload swapping are considered. If the number of vehicles at a DP is limited (e.g., due to limited space or economic reasons), the flight demand needs to be shifted to handle all requests. This will ultimately influence the $\bar{\Phi}$ and Φ_{max} and the FANET metrics accordingly.

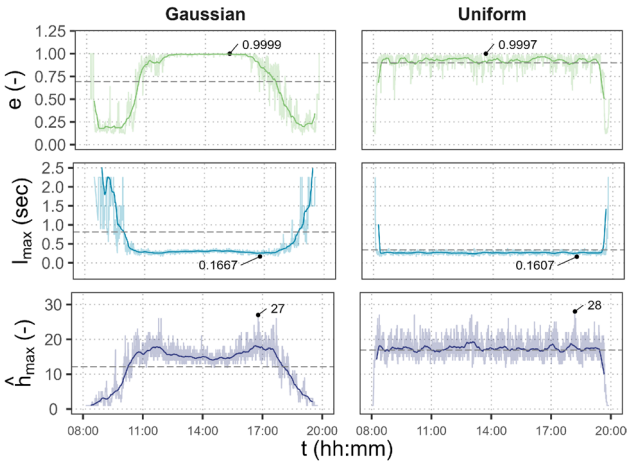

Fig. 22 Exemplary time series for $\hat{h}_{max}(t)$, $l_{max}(t)$ and $e(t)$ ($r_c = 4\,km$; $f_{pd} = 0.005$; vehicle A)

3.2.2 Influence of district size and UAS speed

As in this study, it is assumed that a DP only delivers packages within its delivery district, the size of the districts influences the flight duration. Figure 18 shows box plots for three different maximum district sizes A^D_{max} and for vehicles A and B. It can be observed that as expected, with larger districts, the distribution of mission times shifts toward higher values. Larger mission times in turn lead to higher values of Φ_{max} and $\bar{\Phi}$.

Not only district size but also the speed of aircraft determines the mission time. In Fig. 18, it can be observed that the faster vehicle B leads to lower values of d_m. Hence, in as the cruise speed of vehicle B is much higher than that of vehicle A, in Fig. 16, the curves are flatter than the curves for vehicle A. The UAS can complete their missions faster. Accordingly, slower speeds lead to higher values of Φ_{max} and $\bar{\Phi}$.

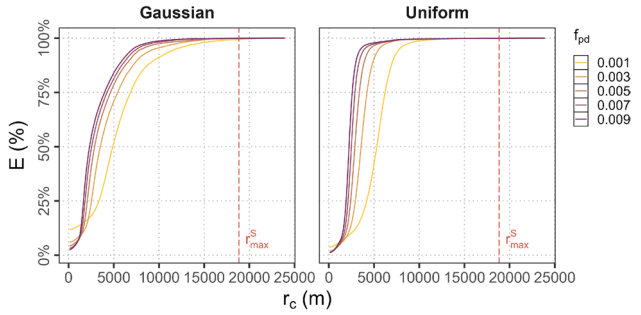

Fig. 23 Dependency of reachability E on communication range r_c for different demand factors f_{pd} for Gaussian and uniform distribution

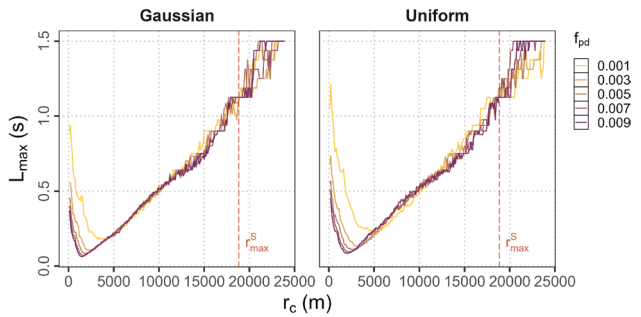

Fig. 24 Dependency of delay budget L_{max} on communication range r_c for different demand factors f_{pd} for Gaussian and uniform distribution

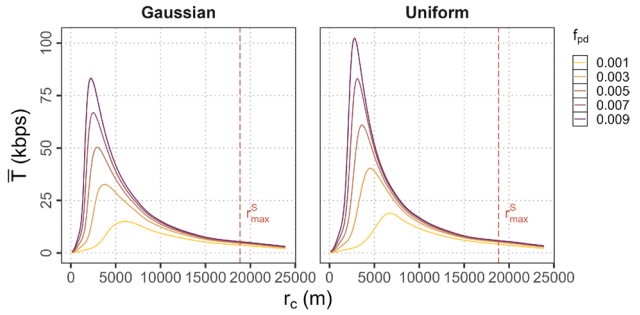

Fig. 25 Dependency of aggregated data rate $\bar{T}$ on communication range r_c for different demand factors f_{pd} for Gaussian and uniform distribution

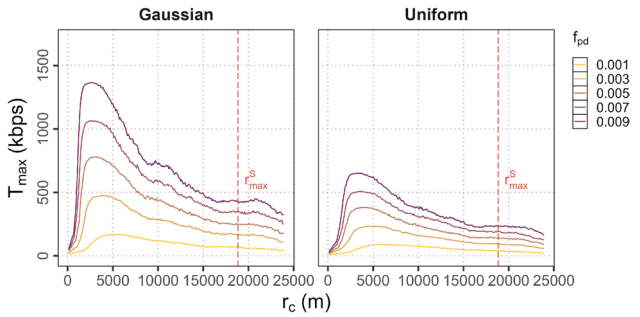

Fig. 26 Dependency of peak data rate T_{max} on communication range r_c for different demand factors f_{pd} for Gaussian and uniform distribution

3.2.3 Aggregated analysis

In a next step, an aggregated analysis of the scenario metrics will be presented. Figure 19 shows the values for Φ_{max} and $\bar{\Phi}$ (left axis) and for the aggregated geographic densities $\bar{\Delta}_g$ and Δ_{gmax} (right axis) for different demand factors f_{pd} and vehicles A and B. The relation is linear, while the slope of the linear fit is dependent on the city geometry under evaluation as well as on the vehicle type.

Figure 20 shows similar to Fig. 19 a combined plot for the aggregated metrics for different district sizes A^D_{max}. As can be expected, due to the change in average mission time resulting from larger district sizes, the values for mean and peak values increase accordingly.

3.2.4 Linear model fit

In a next step, we fit linear models of the form

$$\bar{\Delta}_g, \Delta_{\text{gmax}} = f(f_{\text{pd}}, \bar{A}^D) \tag{23}$$

to the specific scenario data (fixed city and vehicle).

More general models could be derived in future works including varying city sizes A^S and average vehicle speeds $\bar{v}_{\text{uas}}$. Using the linear model, we can then estimate the demand factor that will lead to a certain aggregated UAS density $\bar{\Delta}_g$.

For City A as assumed in this work, Table 2 resumes the values obtained by the model. It can be seen that an aggregated geographic UAS density of $\bar{\Delta}_g = 1/\text{km}^2$ for vehicle A and an uniform demand distribution is obtained if a demand factor of about 20 packages per 1000 inhabitants is reached. Similar values are obtained for uniform distribution. A peak number of simultaneous operating vehicles of $\Phi_{\text{max}} = 1000$ is obtained for 20 packages per 1000 inhabitants for uniform demand distribution, in contrast to the Gaussian distribution, that reaches this value with only about half the number of packages.

3.3 FANET analysis

Finally, we apply the graph-search-based FANET assessment to the generated UAS trajectories to obtain time series for each of the FANET metrics. Exemplary results for a fixed setting ($f_{\text{pd}} = 0.005$ and $r_c = 4$ km) are shown in Fig. 21 and 22.

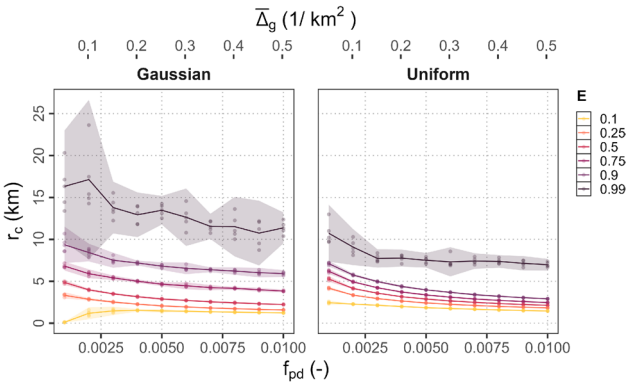

Fig. 27 Required communication range r_c for different reachability levels E against demand factor f_{pd} (lower axis) and aggregated density $\bar{\Delta}_g$ (upper axis) for Gaussian and uniform distribution

In this configuration, at most times of the day around 15 hops are required for data to traverse the entire network, resulting in a delay budget $l_{\max}$ of around 150 ms for both Gaussian and uniformly distributed UAS traffic. Nevertheless, the highest number of hops $\hat{h}_{\max}$ observed is 28 for Gaussian distributed traffic, demanding a $l_{\max}$ of less than 170 ms. Comparing the two traffic distributions, significant differences can be observed for $e(t)$ and data rate. Especially in the early morning and late evening, $e(t)$ for Gaussian distributed traffic remains lower than 50%. The highest peak data rate $\tau_{\max}(t)$ required here (750 kbps) is more than twice the highest value observed for uniformly distributed traffic.

3.3.1 Influence of communication range

The achievable aggregated reachability E is displayed in Fig. 23. As expected, E grows with increasing communication range. We can also observe that a higher demand factor generally results in a lower required communication range for the same reachability E.

Comparing Gaussian and uniformly distributed flight demand, we can see that uniform demand results in higher values for the reachability E. This can be attributed to the fact that in the early morning and late evening hours in the

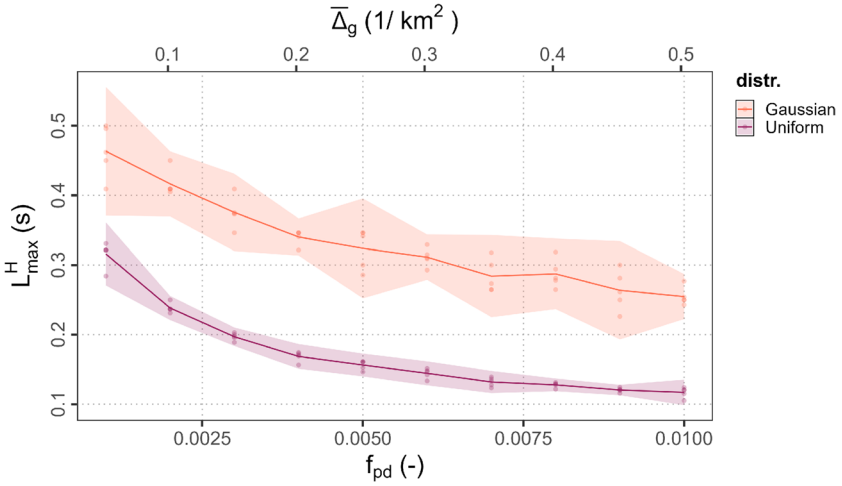

Fig. 28 Delay budget $L^H_{\max}$ for a 90% reachability against demand factor f_{pd} (lower axis) and aggregated density $\bar{\Delta}_g$ (upper axis) for Gaussian and uniform distribution

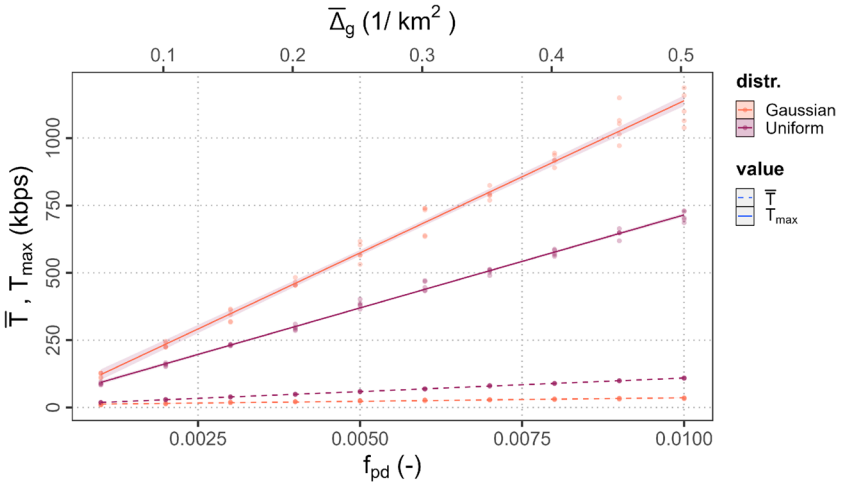

Fig. 29 Peak and average data rate $T_{\max}$ and $\bar{T}$ for a 90% reachability against demand factor f_{pd} (lower axis) and aggregated density $\bar{\Delta}_g$ (upper axis) for Gaussian and uniform distribution

uniform case, the network is better connected as more vehicles are airborne.

The delay budget is shown in Fig. 24. For low communication ranges, very high delay budgets can be observed, as the network is poorly connected and data are only forwarded over a few hops. Increasing the communication range improves the connectivity, so that data are forwarded over many hops and consequently the delay budget decreases. For a high demand factor ($f_{\mathrm{pd}} = 0.01$), the delay budget reaches a minimum of 60 ms. Increasing the communication range even further results in a linear increase of the delay budget again as now fewer hops are required to traverse the entire network. In this region of communication range, the delay budget does not depend on the demand factor any more but is only determined by the outer network dimensions.

The resulting data rates are shown in Figs. 25 and 26. Again, we observe the same phenomenon as for the delay. For low communication ranges, the network is poorly connected and only a low data rate is required to deliver the data. Once the communication range allows for forwarding over many hops, the aggregated data rate increases drastically reaching a peak of more than 112 kbps. As the communication range increases further, the data rate is lowered again as data have to be forwarded over fewer hops.

We can also observe a strong difference between the aggregated and the peak data rate. Especially, in poorly connected networks, many forwarding paths go through the same few UAS that consequently require a very high peak data rate of up to 1477 kbps. While this effect persists for higher communication ranges, it becomes less pronounced.

3.3.2 Aggregated analysis

Using these results, we can also analyze the FANET performance from an application requirement perspective. For example, Fig. 27 shows the required communication range for a given reachability E and demand factor. We can see that in general, a higher communication range is required to reach a higher E. This effect is especially visible for low demand factors and Gaussian demand distribution, where an E of 90% requires almost 10 km communication range but an E of 99% more than 15 km.

Assuming that a 90% reachability is sufficient for our applications, we can further take the required communication range and obtain the other metrics.

The delay budget is shown in Fig. 28. Again, we see a trend, where a low demand factor allows for a high delay budget. If the traffic is Gaussian distributed, the delay budget is roughly 150 ms higher than for uniformly distributed traffic over all demand factors.

The data rate displayed in Fig. 29 has a linear dependence on the demand factor. However, while the average data rate only increases slowly with the demand factor, the peak data rate increases more than ninefold between a demand factor of 0.001 and 0.01. The results also show that Gaussian distributed traffic requires a slightly lower $\bar{T}$ than uniformly distributed traffic, at the cost of a substantially higher T_{max}.

4 Conclusion and outlook

In the work presented in this paper, we showed that FANET performance is highly dependent on number and position of communication nodes. Both factors are strongly influenced by city geometry, number of droneports, flight demand pattern/distribution, vehicle speed, and more. We presented a modeling approach to create UAS flight movements for generic cites that can be constructed using basic parameters. For a thereby created city matching area and population of Hamburg, we showed with our modeling approach that a flight demand of 5 packages per 1000 inhabitants per day results in 490 UAS in the air at peak times and 190 on average for a Gaussian demand distribution. Uniform demand distribution generally results in lower values. For the city under evaluation, the above values translate to a geographic drone density of 0.648 drones/km^2 in peak times and 0.252 in average. These values linearly scale with the demand factor and are influenced by UAS speed, district size, demand distribution, and more. Using the corresponding linear models, it was calculated that to reach drone densities of 1 drones/km^2, a demand factor of more than 20 packages per thousand inhabitants per day is necessary for both uniform and Gaussian demand distribution. To obtain a maximum value of 1000 simultaneous active UAS, more than 20 packages per thousand inhabitants per day are needed for uniform and about 10 for Gaussian distribution.

Further, we assessed a flooding application for the FANET using the 4D-trajectory data of the simulation. We showed that for the Gaussian demand distribution especially in the morning and evening, penalties for FANET performance occur. From an FANET point of view, it is, therefore, desirable to have a uniform distribution of traffic. We also show that, although peak and average data rates both scale linearly with the demand factor, the peak data rate is many times higher than the average data rate as the FANET topology requires a few nodes to handle a large share of the data traffic. Even for high demand factors or low reachability levels, a communication range of multiple km is required. While this is a challenge for most modern communication systems, potentially requiring special purpose transceivers

and antennas, the delay budget of more than 60 ms is a rather relaxed requirement.

These insights are useful to select and dimension communication technologies for the scenario at hand. Nevertheless, the numbers only serve as a rough estimate as some important aspects concerning radio performance estimation were not yet considered, such as line-of-sight effects and atmospheric fading. Hence, our approach cannot replace the need for an in-depth network simulation including channel modeling and medium access protocols which is planned for future work.

In addition, due to the stochastic nature of our approach, only statistic statements can be given. While this might be an disadvantage in terms of specific city analysis on the one hand, on the other hand, it can be an advantage in terms of generalization. While starting with a simple set of parameters describing a city, adding more parameters in the future can lead to better classification of cities and yield more reliable results.

In this context, as only one exemplary city was analyzed in our work, it will be worthwhile to extend the study in the future to cover more cities including varying geometry samples, different city areas, as well as population size and distributions.

Also, different business models (e.g., delivery over district borders, delivery to low density areas) or other UAS applications (e.g., transport of medical goods or inspection of infrastructure) are desirable to be included in the analysis. Further, a vehicle mix, UAS limitations to drone ports, and conflict analysis are interesting areas that are worthwhile to be addressed in the future.

Author contributions Conceptualization: Tobias Marks; methodology: Tobias Marks and Konrad Fuger; data curation: Tobias Marks and Konrad Fuger; software: Tobias Marks and Konrad Fuger; formal analysis and investigation: Tobias Marks; writing—original draft preparation: Tobias Marks; writing—review and editing: Konrad Fuger; funding acquisition: Tobias Marks

Funding Open Access funding enabled and organized by Projekt DEAL. The work presented in this paper was part of the project VEREDUS that was funded by the German Ministry of Economic Affairs and Climate Action (BMWK) under the National Aeronautical Research Program (LuFo) V-3 under the Grant Agreement No. 20Q1939H.

Availability of data and materials All data that are not subject to licensing agreements by third parties can be made available by the corresponding author upon reasonable request.

Code availability The software code is proprietary information of the German Aerospace Center (DLR). Therefore, the code cannot be made available to the public or the readers without any restrictions. The codes used for analyzing the data and plotting the analyzed data are available from the corresponding author upon reasonable request.

Declarations

Conflict of interest The authors have no relevant financial or non-financial interests to disclose.

Ethics approval Not applicable.

Consent to participate Not applicable.

Consent for publication All authors expressed their consent for this publication.

References

1. Zeng, Y., Zhang, R., Lim, T.J.: Wireless communications with unmanned aerial vehicles: opportunities and challenges. IEEE Commun. Mag. **54**(5), 36–42 (2016). https://doi.org/10.1109/MCOM.2016.7470933
2. Matracia, M., Kishk, M.A., Alouini, M.-S.: UAV-aided post-disaster cellular networks: a novel stochastic geometry approach. IEEE Trans. Veh. Technol. **72**(7), 9406–9418 (2023)
3. Benarbia, T., Kyamakya, K.: A literature review of drone-based package delivery logistics systems and their implementation feasibility. Sustainability (2022). https://doi.org/10.3390/su14010360
4. European Commission.: Commission Delegated Regulation (EU) 2019/945 of 12 March 2019 on unmanned aircraft systems and on third-country operators of unmanned aircraft systems. Technical report (2019)
5. European Commission.: Commission Implementing Regulation (EU) 2019/947 of 24 May 2019 on the rules and procedures for the operation of unmanned aircraft. Technical report (2019)
6. OECD and European Commission.: The Shape of Cities and Sustainable Development (2020). https://doi.org/10.1787/165ea317-en. https://www.oecd-ilibrary.org/content/component/165ea317-en
7. Fuger, K., Marks, T., Kuladinithi, K., Timm-Giel, A.: Modeling of communication requirements for distributed UTM using stochastic geometry. In: 2024 IEEE International Conference on Pervasive Computing and Communications Workshops and Other Affiliated Events (PerCom Workshops), pp. 666–671 (2024). IEEE
8. Fuger, K., Kuladinithi, K., Sood, M., Timm-Giel, A.: Feasibility study on position verification in urban UAV networks. In: 2023 33rd International Telecommunication Networks and Applications Conference, pp. 38–43 (2023). IEEE
9. Fuger, K., Timm-Giel, A.: On the feasibility of position-flooding in urban UAV networks. In: 2023 IEEE 97th Vehicular Technology Conference (VTC2023-Spring), pp. 1–5 (2023). IEEE
10. Marks, T., Fuger, K.: Mutual position plausibility checking in flying ad-hoc networks using distance measurements. In: ICAS

Proceedings 2024. The International Council of the Aeronautical Sciences (2024)
11. Khan, M.A., Safi, A., Qureshi, I.M., Khan, I.U.: Flying ad-hoc networks (FANETs): a review of communication architectures, and routing protocols. In: 2017 First International Conference on Latest Trends in Electrical Engineering and Computing Technologies (INTELLECT), pp. 1–9 (2017). IEEE
12. Wheeb, A.H.: Flying ad hoc networks (FANET): performance evaluation of topology based routing protocols. Int. J. Interact. Mob. Technol **16**(4), 137–149 (2022)
13. Rosati, S., Krużelecki, K., Traynard, L., Mobile, B.R.: Speed-aware routing for uav ad-hoc networks. In: 2013 IEEE Globecom Workshops (GC Wkshps), pp. 1367–1373 (2013). IEEE
14. Liang, B., Haas, Z.J.: Predictive distance-based mobility management for pcs networks. In: IEEE INFOCOM '99. Conference on Computer Communications. Proceedings. Eighteenth Annual Joint Conference of the IEEE Computer and Communications Societies. The Future Is Now (Cat. No.99CH36320). IEEE. https://doi.org/10.1109/infcom.1999.752157
15. Biomo, J.-D.M.M., Kunz, T., St-Hilaire, M.: An enhanced Gauss–Markov mobility model for simulations of unmanned aerial ad hoc networks. In: 2014 7th IFIP Wireless and Mobile Networking Conference (WMNC), pp. 1–8 (2014). https://doi.org/10.1109/WMNC.2014.6878879
16. Johnson, D.B., Maltz, D.A.: Dynamic Source Routing in Ad Hoc Wireless Networks, pp. 153–181. Springer. https://doi.org/10.1007/978-0-585-29603-6_5
17. Wan, Y., Namuduri, K., Zhou, Y., He, D., Fu, S.: A smooth-turn mobility model for airborne networks. In: Proceedings of the First ACM MobiHoc Workshop on Airborne Networks and Communications. MobiHoc '12. ACM. https://doi.org/10.1145/2248326.2248333
18. Chriki, A., Touati, H., Snoussi, H., Kamoun, F.: Fanet: communication, mobility models and security issues. Comput. Netw. **163**, 106877 (2019)
19. Kumari, K., Sah, B., Maakar, S.: A survey: different mobility model for fanet. Int. J. Adv. Res. Comput. Sci. Softw. Eng. **5**(6) (2015)
20. Zolanvari, M., Jain, R., Salman, T.: Potential data link candidates for civilian unmanned aircraft systems: A survey. IEEE Commun. Surv. Tutor. **22**(1), 292–319 (2019)
21. SESAR Joint Undertaking.: European Drones Outlook Study Unlocking the value for Europe. Technical report (2016). https://doi.org/10.2829/085259
22. The Canberra Times.: Wing's drone delivery service is about more than just flying takeout (2022). https://www.canberratimes.com.au/story/7802239/drone-delivery-is-about-more-than-just-flying-takeout/
23. China Daily.: Meituan's UAV delivery service wows visitors (2023). https://www.chinadaily.com.cn/a/202302/22/WS63f57174a31057c47ebb01da.html
24. Doole, M., Ellerbroek, J., Hoekstra, J.: Drone delivery: urban airspace traffic density estimation. In: In Proceedings of Eight SESAR Innovation Days Conference (2018)
25. Doole, M., Ellerbroek, J., Hoekstra, J.: Estimation of traffic density from drone-based delivery in very low level urban airspace. J. Air Transp. Manag. **88**, 101862 (2020)
26. Borghetti, F., Caballini, C., Carboni, A., Grossato, G., Maja, R., Barabino, B.: The use of drones for last-mile delivery: a numerical case study in Milan, Italy. Sustainability (2022). https://doi.org/10.3390/su14031766
27. Swaid, M., Lau, A., Linke, F.: U-Space modeling and efficiency evaluation in the city of Hamburg (2023). https://doi.org/10.2514/6.2023-3333
28. Kirschstein, T.: Comparison of energy demands of drone-based and ground-based parcel delivery services. Transp. Res. Part D Transp. Environ. **78**, 102209 (2020). https://doi.org/10.1016/j.trd.2019.102209
29. Hu, B., Brandstätter, G., Müller, J., Stern, P., Schaffenberger, A., Fallast, A., Lesak, S., Meinhard, D.: Assessing automated air-taxis for urban mobility. Eur. Transp. Res. Rev. (2024). https://doi.org/10.1186/s12544-024-00658-w
30. Parish, Y.I.H., Müller, P.: Procedural modeling of cities. In: In Proceedings of the 28th Annual Conference on Computer Graphics and Interactive Techniques. SIGGRAPH '01, pp. 301–308. Association for Computing Machinery (2001). https://doi.org/10.1145/383259.383292
31. Kelly, G., McCabe, H.: A survey of procedural techniques for city generation, vol. 14 (2006)
32. Terekhov, I.: Assessing noise effects of the urban air transportation system (2018). https://doi.org/10.2514/6.2018-2954
33. Patterson, M.D., Antcliff, K.R., Kohlman, L.W.: A proposed approach to studying urban air mobility missions including an initial exploration of mission requirements. In: 75th Annual Forum and Technology Display (2018)
34. Yang, X., Deng, L., Liu, J., Wei, P., Li, H.: Multi-agent autonomous operations in urban air mobility with communication constraints. In: AIAA Scitech 2020 Forum (2020). https://doi.org/10.2514/6.2020-1839
35. Asmer, L., Jaksche, R., Pak, H., Kokus, P.: A city-centric approach to estimate and evaluate global urban air mobility demand. https://doi.org/10.1007/s13272-024-00742-w
36. Dahle, O.H., Rydberg, J., Dullweber, M., Peinecke, N., Bechina, A.A.A.: A proposal for a common metric for drone traffic density. In: 2022 International Conference on Unmanned Aircraft Systems (ICUAS), pp. 64–72 (2022). https://doi.org/10.1109/ICUAS54217.2022.9836143
37. Drone Delivery Canada.: DDC announces approval for commercial BVLOS drone delivery operations for UBC'S remote communities DTI program (2022). https://dronedeliverycanada.com/press-releases/ddc-announces-approval-for-commercial-bvlos-drone-delivery-operations-for-ubcs-remote-communities-dti-program/
38. Kellermann, R., Biehle, T., Fischer, L.: Drones for parcel and passenger transportation: a literature review. Transp. Res. Interdiscip. Perspect. **4**, 100088 (2020). https://doi.org/10.1016/j.trip.2019.100088
39. Hamissi, A., Dhraief, A.: A survey on the unmanned aircraft system traffic management. ACM Comput. Surv. **56**(3), 1–37 (2023)
40. European Commission.: Commission Implementing Regulation (EU) 2021/664 of 22 April 2021 on a regulatory framework for the U-space. Technical report (2021)
41. ICAO.: Guidance Material on Comparison of Surveillance Technologies (GMST). OCLC: 1135358455. ICAO (2007)
42. MAVLINK.: MAVLINK Common Message Set. https://mavlink.io/en/messages/common.html
43. ICAO.: ADS-B Implementation and Operations Guidance Document (AIGD). Edition: 14.0. ICAO (2021)
44. Peinecke, N.: How to stay well clear in corridors and swarms: detect-and-avoid ranges for geovectoring concepts. In: 2022 International Conference on Unmanned Aircraft Systems (ICUAS), pp. 57–63 (2022). IEEE
45. Füßler, H., Widmer, J., Käsemann, M., Mauve, M., Hartenstein, H.: Contention-based forwarding for mobile ad hoc networks. Ad Hoc Netw. **1**(4), 351–369 (2003)